Available online at www.sciencedirect.com
SCIENCE DIRECT®
Remote Sensing of Environment 89 (2004) 309–325
Remote Sensing of Environment
www.elsevier.com/locate/rse

Sea–air flux of CO_2 in the Caribbean Sea estimated using in situ and remote sensing data

Are Olsen[a,b,*], Joaquin A. Triñanes[c], Rik Wanninkhof[d]

[a] Geophysical Institute, University of Bergen, Allégaten 70, 5007 Bergen, Norway
[b] Bjerknes Centre for Climate Research, Allégaten 55, 5007 Bergen, Norway
[c] Cooperative Institute for Marine and Atmospheric Studies, University of Miami, Miami, Florida, USA
[d] NOAA/Atlantic Oceanographic and Meteorological Laboratory, Miami, Florida, USA

Received 24 June 2003; received in revised form 17 October 2003; accepted 23 October 2003

Abstract

Empirical relationships between sea surface carbon dioxide fugacity (fCO_2^{sw}) and sea surface temperature (SST) were applied to datasets of remotely sensed SST to create fCO_2^{sw} fields in the Caribbean Sea. SST datasets from different sensors were used, as well as the SST fields created by optimum interpolation of bias corrected AVHRR data. Empirical relationships were derived using shipboard fCO_2^{sw} data, in situ SST data, and SST data from the remote sensing platforms. The results show that the application of a relationship based on shipboard SST data, on fields of remotely sensed SST yields biased fCO_2^{sw} values. This bias is reduced if the fCO_2^{sw}–SST relationships are derived using the same SST data that are used to create the SST fields. The fCO_2^{sw} fields found to best reproduce observed fCO_2^{sw} are used in combination with wind speed data from QuikSCAT to create weekly maps of the sea–air CO_2 flux in the Caribbean Sea in 2002. The region to the SW of Cuba was a source of CO_2 to the atmosphere throughout 2002, and the region to the NE was a sink during winter and spring and a source during summer and fall. The net uptake of CO_2 in the region was doubled when potential skin layer effects on fCO_2^{sw} were taken into account.

Keywords: Caribbean Sea; Carbon dioxide; Air–sea flux; Remote sensing; AVHRR; MODIS; TMI; Sea surface temperature

1. Introduction

The Ocean Carbon Watch project is an initiative of the National Oceanic and Atmospheric Administration (NOAA) in the USA that aims to routinely produce monthly to seasonal sea–air CO_2 flux maps for the ocean regions bordering the North American continent. Such maps will be valuable for a number of reasons. They will better constrain the sea–air flux of CO_2 in these areas. Over longer timescales, the maps will also allow for estimates of interannual variability in the flux and identification of factors driving such variations. Such maps will also better constrain atmospheric inversion estimates of the North American terrestrial carbon sink.

Production of sea–air CO_2 flux maps requires a high-density observation network that measures the fugacity of carbon dioxide in surface water (fCO_2^{sw}). However, the number of observations and their frequency can be significantly reduced if robust methods for spatial and temporal interpolation of available fCO_2^{sw} data are devised. A promising approach in this respect is the application of empirical relationships between fCO_2^{sw} and sea surface temperature (SST), on fields of remotely sensed SST (Cosca et al., in press; Goyet et al., 1998; Hood, Merlivat, & Johannessen, 1999; Lee, Wanninkhof, Takahashi, Doney, & Feely, 1998; Nelson, Bates, Siegel, & Michaels, 2001; Olsen, Bellerby, Johannessen, Omar, & Skjelvan, in press; Stephens, Samuels, Olson, Fine, & Takahashi, 1995). In this paper, we describe the development and application of such a protocol to produce weekly sea–air CO_2 flux maps for 2002 for the Caribbean Sea region, one of the Ocean Carbon Watch test beds.

The Caribbean Sea (Fig. 1) is a marginal sea adjacent to central and South America and separated from the western North Atlantic subtropical gyre by the Antilles Island arc. The Caribbean Sea is mainly fed by water from the Atlantic subtropical gyre, receiving approximately 17 Sv through the Greater Antilles and Leeward Islands passages (Johns, Townsend, Fratantoni, & Wilson, 2002). An additional 10 Sv enters through the Windward Islands passages. Water exits the Caribbean Sea through the Straits of Florida,

* Corresponding author. Tel.: +47-55-58-43-22; fax: +47-55-58-43-30.
E-mail address: are@gfi.uib.no (A. Olsen).

0034-4257/$ - see front matter © 2003 Elsevier Inc. All rights reserved.
doi:10.1016/j.rse.2003.10.011

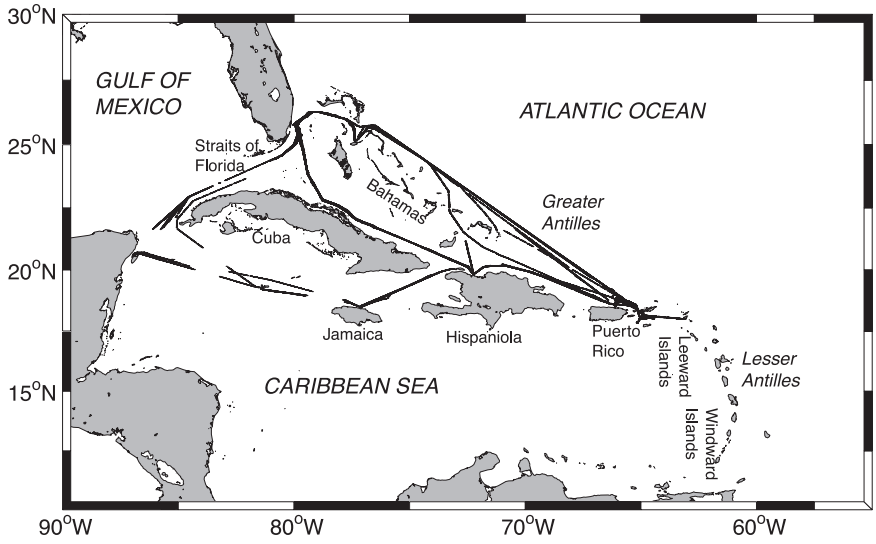

Fig. 1. Map of the Caribbean Sea. The lines show the cruise tracks of the *Explorer of the Seas* where fCO_2^{sw} data were obtained. The eastern cruise track of the *Explorer* goes from Miami to St. Thomas and back again. The western track follows: Miami, Hispaniola, Jamaica, Yucatan Peninsula, and back to Miami.

feeding the Florida Current which has a mean transport of about 30 Sv. The surface ocean CO_2 chemistry of the Caribbean Sea has not been previously described. The region is mostly oligotrophic (Corredor & Morell, 2001; Richards & Bohnsac, 1990) and shows similarities with the subtropical gyre from which it receives most of its water. As detailed by both Lefèvre and Taylor (2002) and Nelson et al. (2001), subtropical gyre fCO_2^{sw} can be fairly well reproduced using SST data.

The fCO_2^{sw} data used in the present work have been obtained from the cruise ship *Explorer of the Seas* which is operated by Royal Caribbean International. The *Explorer* was put in operation in October 2000 and does weekly roundtrips in the Caribbean Sea from Miami, FL, alternating on a western and eastern cruise track (Fig. 1). The ship is equipped with meteorological and oceanographic instruments maintained by the University of Miami's Rosenstiel School of Marine and Atmospheric Science and the NOAA/Atlantic Oceanographic and Meteorological Laboratory (AOML) (Williams, Prager, & Wilson, 2002). The underway fCO_2^{sw} analyzer on board the *Explorer* was installed in February 2002.

We use the fCO_2^{sw} data obtained on board the *Explorer* in 2002 to create an empirical relationship between fCO_2^{sw} and SST. This relationship is then applied to fields of remotely sensed SST providing spatial fields of fCO_2^{sw} which in combination with surface wind speed data from the SeaWinds instrument on the QuikSCAT satellite are used to compute sea–air CO_2 flux fields. An important part of this effort focuses on reducing bias in the computed fCO_2^{sw} fields resulting from biases in the remotely sensed SST data. The accuracy and validation of remotely sensed SST data have been the subject of numerous studies. For instance, SST data retrieved by the Advanced Very High Resolution Radiometer (AVHRR) sensors on board the polar orbiting NOAA-12 and NOAA-14 satellites have been found to be biased low by 0.4 °C during day and 0.2 °C during night when compared to buoy SST in the Gulf of Mexico (Li, Pichel, Clemente-Colón, Krasnopolsky, & Sapper, 2001a). If the slope of the fCO_2^{sw}–SST regression is close to the thermodynamic effect of $\delta \ln fCO_2/\delta T = 0.0423\ ^\circ C^{-1}$ (Takahashi, Olafsson, Goddard, Chipman, & Sutherland, 1993) as observed in the subtropical gyre (Lefèvre & Taylor, 2002, this study), then at a fCO_2^{sw} level of 340 ppm typical for the Caribbean Sea, such a bias in remotely sensed SST corresponds to nearly 6 μatm in fCO_2^{sw}. Hence, one important issue is whether one should apply fCO_2^{sw}–SST relationships based only on shipboard data on remotely sensed SST fields, or if it is better to apply fCO_2^{sw}–SST relationships based on shipboard fCO_2^{sw} and remotely sensed SST data.

This issue is addressed by comparing a fCO_2^{sw}–SST relationship based on in situ data only, with relationships based on in situ fCO_2^{sw} data and collocated remotely sensed SST data. We formulate a set of four fCO_2^{sw}–SST relationships based on fCO_2^{sw} data from the *Explorer* and: (1) shipboard SST data from the thermosalinograph on board the *Explorer*, (2) collocated SST from the AVHRR on board the NOAA Polar Operational Environmental Satellites (POES), (3) collocated SST data from the Moderate Resolution Imaging Spectroradiometer (MODIS) on board the NASA Earth Observing System (EOS) Terra satellite, and (4) collocated SST data from the Tropical Rainfall Measuring Mission (TRMM) Microwave Imager (TMI). Each of the three latter relationships is then applied to fields of SST computed using data from the sensor used to create the relationships, and the resulting fCO_2^{sw} values are compared with the fCO_2^{sw} values computed by applying the equation derived from shipboard fCO_2^{sw} and SST data on the same fields. We also compute fCO_2^{sw} fields from the analyzed fields of bias corrected satellite SST produced by NOAA

using optimum interpolation (Reynolds, Rayner, Smith, Stokes, & Wang, 2002) and the equation derived from shipboard data. This evaluation is carried out in Section 2.

Maps of the fCO_2^{sw} distribution in the Caribbean Sea are presented along with the corresponding sea–air CO_2 flux fields in Section 3.

The algorithm developed in Section 2 is optimized to reproduce fCO_2^{sw} at the SST determined by the thermosalinograph on board the *Explorer* that has an intake depth of two m. As pointed out by Robertson and Watson (1993), use of fCO_2^{sw} at 2 m depth to compute the sea–air CO_2 flux may bias the flux because of the existence of a cool skin layer at the sea surface. We address this issue by developing an empirical relationship that reproduces fCO_2^{sw} at the skin temperature as determined by a Marine-Atmospheric Emitted Radiance Interferometer (M-AERI) (Minnett et al., 2001) on board the *Explorer*. We also discuss the effect of diurnal covariance between wind speed and SST on the sea–air CO_2 flux estimate, and the effect of using monthly resolution instead of weekly. This is carried out in the discussion part of this paper (Section 4).

2.. Data and calculations

2.1. Field measurements

The field data used in this study have been collected on board the cruise ship *Explorer of the Seas*. Seawater is drawn from an intake at 2 m depth and distributed through a manifold to different sensors. The thermosalinograph (Seabird) is located close to the intake in the bow thruster room. The underway fCO_2^{sw} system is located in the oceanographic laboratory amidships on a lower deck. It is patterned after and operates under principles similar to those described in Feely et al. (1998) and Wanninkhof and Thoning (1993). Main differences with the units referenced are a smaller equilibrator, the method of drying the gas, and absence of marine air measurements. The equilibrator consists of a small (1.2 l) equilibrator in which seawater is sprayed at 1.5 l min^{-1}. The spray causes rapid equilibration of the CO_2 in the seawater with the headspace. The headspace of the equilibrator is isolated from lab air except for vents on the main chamber and on the overflow drain that is sealed from the 0.6 l headspace with a water seal. The vents serve to keep the headspace at ambient pressure which is measured in the laboratory with a precision and accuracy of 0.02 and 0.2 mbar, respectively. The temperature of the water in the equilibrator is measured with a thermistor that is accurate to 0.05 °C through calibration with a NIST traceable thermometer (Hart, thermistor and thermistor module 2563). Even though the fCO_2^{sw} instrument is located at a distance from the intake, temperature changes between the thermosalinograph and equilibrator are generally within 0.5 °C, so that the iso-chemical temperature dependency of Takahashi et al. (1993) of 4.23% C^{-1} can safely be used to adjust the data to the in situ SST. The headspace from the equilibrator is circulated through a Permapure Nafion dryer, to extract all water vapor, and subsequently through an $MgClO_4$ guard column and a 2-μm disk filter prior to entering a LI-COR 6251 nondispersive infrared analyzer. All air is returned to the headspace of the equilibrator. The system is calibrated hourly with three reference standards obtained from NOAA/Climate Monitoring and Diagnostics Laboratory (CMDL) with concentrations of 192.34, 426.96, and 514.24 ppm. The drying gas is a commercially obtained CO_2 in air close to ambient air concentrations of 370 ppm. This gas is also used in the reference channel and is calibrated against the standards at the top of every hour. Other than the 8 min devoted to measuring standards and the reference gas, the hourly cycle is devoted to measuring surface water samples every 2.5 min. Because of the location of the laboratory, it is not possible to draw ambient marine air from the bow for analysis and calculation of sea–air fCO_2 differences as is routinely done with such systems.

Upon analysis of the fCO_2 data acquired in 2002, events of elevated equilibrator headspace fCO_2 levels were encountered. These were unequivocally attributed to an air leak drawing a small amount of ambient air into the equilibrator. Contamination of fCO_2 values appears, however, to have required laboratory air CO_2 concentrations above a certain (unknown) threshold value, reached only when guided tours of the laboratory were carried out. This is based on the regression coefficients of the fCO_2^{sw}–SST relationships in the data. The coefficients remained the same before, during, and after the leak, provided the data obtained during the guided tours in the laboratory and 9.5 h thereafter were removed from the dataset obtained during the leak. Thus, since June the present dataset does not contain any fCO_2^{sw} measurements from approximately 1530 until 0100 h the following day, local time.

2.2. Remotely sensed sea surface temperature data

Remotely sensed SST data from three sources, namely AVHRR, MODIS, and TMI, were used. The AVHRR SST data were provided by the NOAA/National Environmental, Satellite, Data and Information Service (NESDIS) CoastWatch Caribbean Node which generates SST products from the High Resolution Picture Transmission (HRPT) data stream of the NOAA/POES constellation. We use data from the AVHRR/3 sensors aboard the NOAA-15 and NOAA-16 satellites, giving a total of four passes per day (local passing times approximately: 0100–0300, 0600–0800, 1300–1500, and 1800–2000 h). SST has been computed using AVHRR/3 channels 4, 5 and the satellite zenith angle using the NOAA/NESDIS nonlinear multichannel SST algorithm (Li, Pichel, Maturi, Clemente-Colón, & Sapper, 2001b), at a spatial resolution of 1.1 km at nadir. The data have been screened for cloud contaminated cells using the CLouds

from AVhRr (CLAVR) algorithm (Stowe et al., 1991), and resampled to a 2.5-km resolution using a nearest neighbor technique.

The SST data from the MODIS instrument on board the EOS Terra Satellite were provided by the NASA/Goddard Earth Sciences Distributed Active Archive Center (GES DAAC) at http://daac.gsfc.nasa.gov/. We used the long-wave channel (11 μm) SST data, processing version 4. EOS Terra was launched in December 1999 and flies in a near polar orbit with local passing times over the Caribbean Sea at approximately 1000–1200 and 2200–2400 h. We use 5-min orbital swaths at 1 km spatial resolution. The data were screened using the quality flags supplied with the SST data and only pixels of highest quality have been used.

The SST data from the microwave imager on board the TRMM satellite (TMI) were produced by Remote Sensing Systems and sponsored by NASA's Earth Science Information Partnerships (ESIP): a federation of information sites

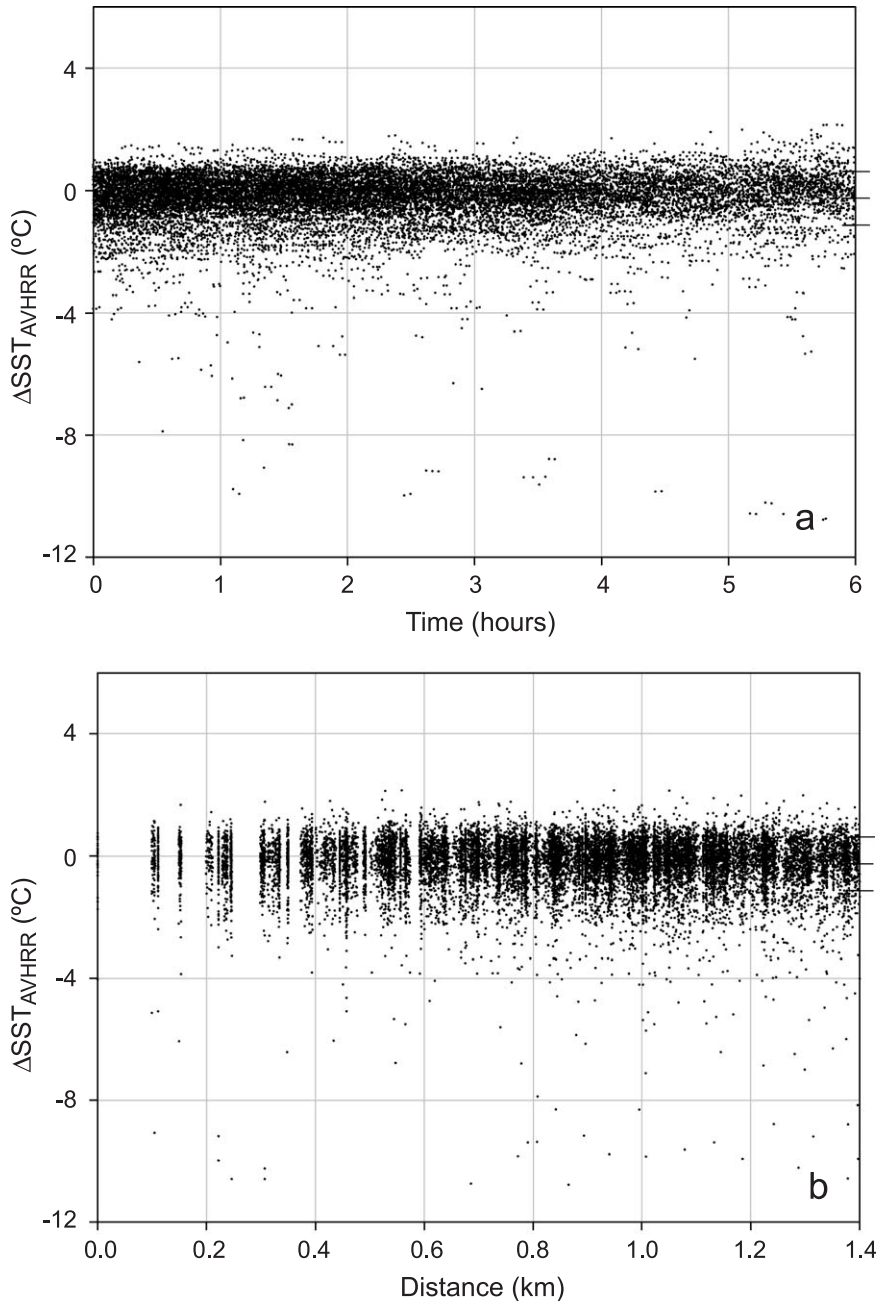

Fig. 2. Difference between sea surface temperatures retrieved by AVHRR and the thermosalinograph on board the *Explorer* ($\Delta SST_{AVHRR} = SST_{AVHRR} - SST_{TSG}$) as a function of the difference in time (a) and space (b) between the measurements. The ticks on the right axis indicate the mean and standard deviation of ΔSST_{AVHRR} of -0.26 ± 0.88 °C.

for Earth Science: and by NASA's TRMM Science Team. The TMI sensor is a multi-channel passive microwave radiometer capable of retrieving both rainfall and SST information including cloud covered regions which is not possible with the MODIS and AVHRR instruments (Wentz, Gentemann, Smith, & Chelton, 2000). The TRMM satellite travels east to west in a semi-equatorial orbit and local passing times varies. We used data from both ascending and descending orbit segments at a resolution of 25 km. All data closer than 50 km from land have been removed from this dataset, in order to minimize the number of land contaminated pixels.

For all sensors, remotely sensed SST data below 15 °C in the Caribbean Sea were considered unrealistic and discarded.

The analyzed fields of bias corrected satellite SST were provided by NOAA/National Center for Environmental Prediction (NCEP)/Environmental Modeling Center (EMC) (http://www.emc.ncep.noaa.gov/research/cmb/sst_analysis/). These global fields are computed on a weekly basis on a 1° latitude (lat) × 1° longitude (lon) spatial resolution following Reynolds et al. (2002), and are created by optimal interpolation of AVHRR SST data that have been adjusted relative to in situ SST from buoy and ship

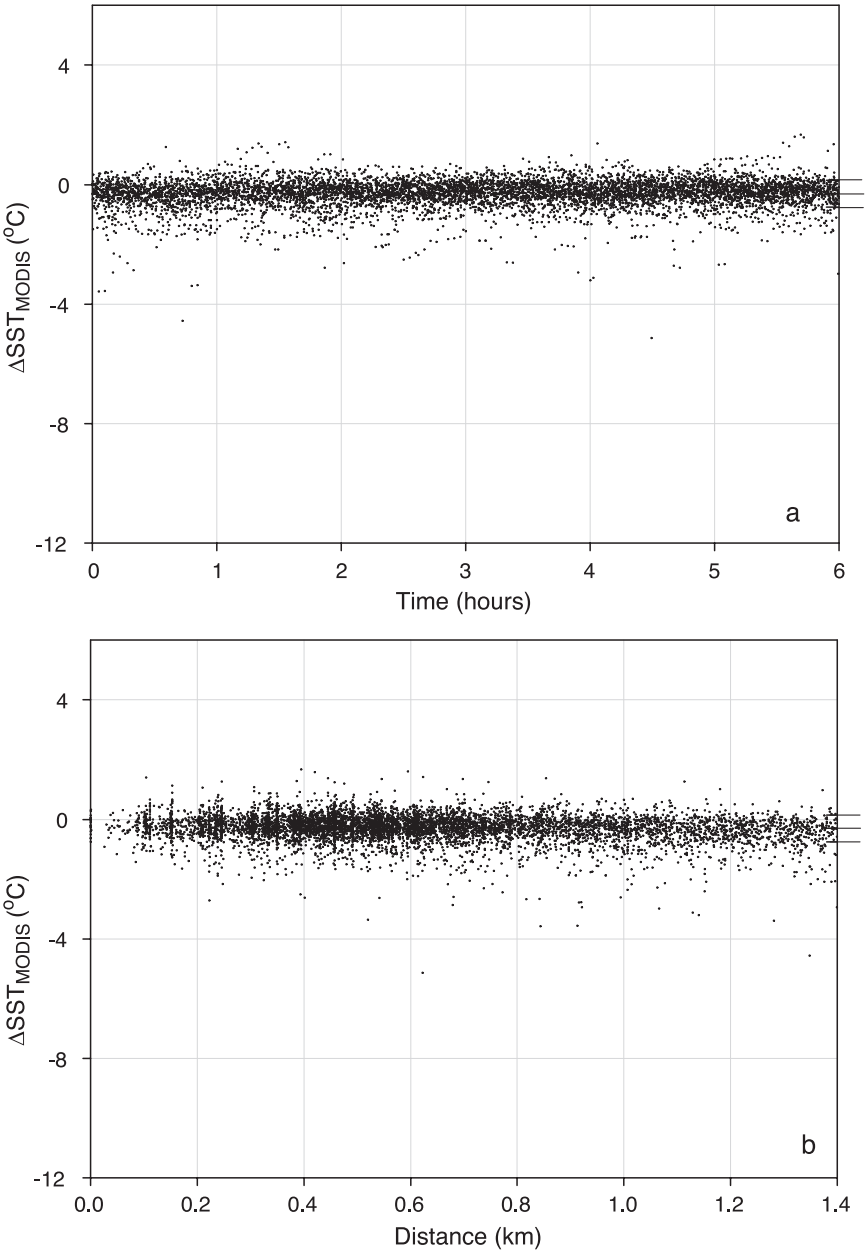

Fig. 3. As Fig. 2, but comparing MODIS sea surface temperature measurements with measurements from the thermosalinograph on board the *Explorer* ($\Delta SST_{MODIS} = SST_{MODIS} - SST_{TSG}$). The mean and standard deviation of ΔSST_{MODIS} are -0.30 ± 0.45 °C.

observations. Henceforth, these data are referred to as the Reynolds SST.

2.3. Estimation of fCO_2^{sw} from remotely sensed SST

Empirical relationships between observed fCO_2^{sw} and SST were employed to compute fCO_2^{sw} from remotely sensed SST. In situ fCO_2^{sw} data were fit to SST data from the thermosalinograph on board the *Explorer*, and also to collocated remotely sensed SST data. In situ fCO_2^{sw} were collocated with AVHRR/MODIS SST data by selecting data from pixels centered within ± 1.4 km from the cruise track and from overpasses within ± 6 h of the time of any fCO_2^{sw} measurement. TMI data were selected by using a temporal cutoff of ± 6 h and a spatial cutoff of ± 4.5 km. Reynolds SST data were not collocated with in situ data because of the relatively coarse resolution of this product.

The temporal and spatial limits for the collocation procedure were determined based on comparison of remotely sensed data with SST data from the thermosalinograph. Fig. 2a and b shows the temperature difference

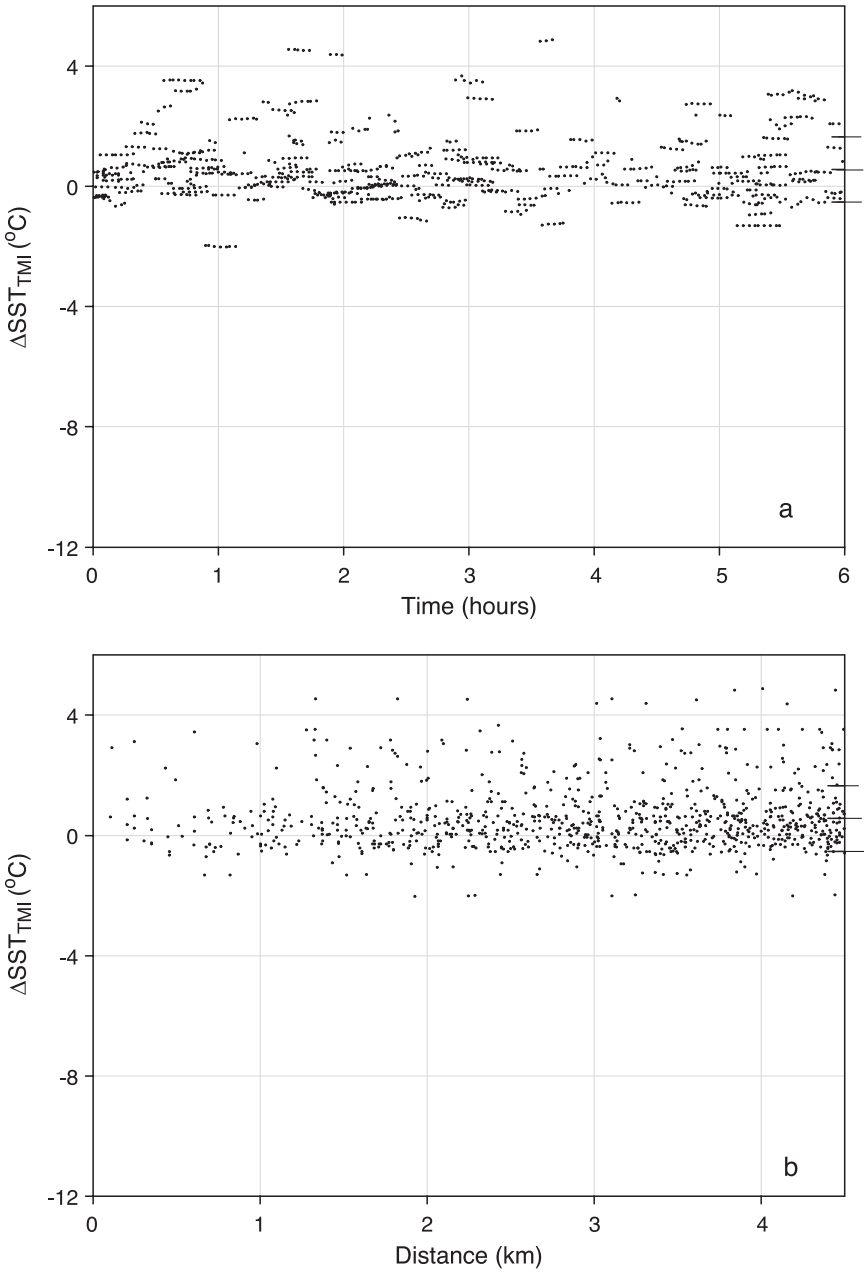

Fig. 4. As Fig. 2, but comparing TMI sea surface temperature measurements with measurements from the thermosalinograph on board the *Explorer* ($\Delta SST_{TMI} = SST_{TMI} - SST_{TSG}$). The mean and standard deviation of ΔSST_{TMI} are 0.56 ± 1.1 °C.

Table 1
Combinations of SST fields (rows) and equations (columns) used to compute fields of fCO_2^{sw}

	Eq. (1)	Eq. (2)	Eq. (3)	Eq. (4)
AVHRR	*	*		
MODIS	*		*	
TMI	*			*
Reynolds	*			

between AVHRR SST and shipboard SST ($\Delta SST_{AVHRR} = SST_{AVHRR} - SST_{TSG}$) as a function of the difference in time and in space, respectively, of the measurements. Fig. 3a and b compares MODIS SST with shipboard SST, and Fig. 4a and b compares collocated TMI SST data with shipboard SST data. Both AVHRR and MODIS SST are biased low compared to the SST from the shipboard TSG at 2 m depth, with a bias of -0.26 ± 0.88 °C ($n = 17610$) and -0.30 ± 0.45 °C ($n = 7020$), respectively. TMI SST on the other hand is biased high, 0.56 ± 1.1 °C ($n = 927$) compared to the shipboard TSG data. The bias remains constant over the temporal and spatial limits chosen as collocation criteria (Figs. 2–4). Since the TMI data are provided at a coarser resolution than the AVHRR and MODIS data, a larger spatial cutoff had to be applied in order to ensure that a sufficient amount of data was available for the fitting procedure. The applied screening methods for the AVHRR retained more low SST data than the screening methods for the MODIS data.

The coefficients for Eqs. (1)–(4) were determined using the computer program SigmaPlot, which employs the Marquardt–Levenberg algorithm (Press, Flannery, Teukolsky, & Vetterling, 1986), minimizing the sum of squares. Because the slope of empirical relationships between fCO_2^{sw} and SST may vary with region (Lefèvre & Taylor, 2002; Nelson et al., 2001), the location of each measurement was also taken into account. Longitude is entered with degrees west as negative values. The regressions are applicable to the region between 15–30°N and 60–90°W. The standard error of each regression coefficient is also given in parenthesis.

For the regression with SST from the TSG:

$$fCO_2^{sw} = 10.18\ (\pm 0.02) \times SST_{TSG} + 0.5249\ (\pm 0.01) \times \text{lat} - 0.2921\ (\pm 0.006) \times \text{lon} + 52.19\ (\pm 0.7)$$
$$n = 40204, \quad r^2 = 0.87, \ \text{rms} = 5.7\ \mu atm. \qquad (1)$$

For the regression with SST from the AVHRR using collocation criteria of less than 1.4 km and less than 6 h:

$$fCO_2^{sw} = 7.328\ (\pm 0.04) \times SST_{AVHRR} - 0.06868\ (\pm 0.04) \times \text{lat} - 0.5680\ (\pm 0.02) \times \text{lon} + 125.1\ (\pm 1)$$
$$n = 17610, \ r^2 = 0.79, \ \text{rms} = 9.5\ \mu atm. \qquad (2)$$

For the regression with SST from the MODIS using collocation criteria of less than 1.4 km and less than 6 h:

$$fCO_2^{sw} = 9.511\ (\pm 0.06) \times SST_{MODIS} + 0.2643\ (\pm 0.04) \times \text{lat} - 0.3923\ (\pm 0.02) \times \text{lon} + 70.98\ (\pm 2)$$
$$n = 7020, \ r^2 = 0.80, \ \text{rms} = 7.6\ \mu atm. \qquad (3)$$

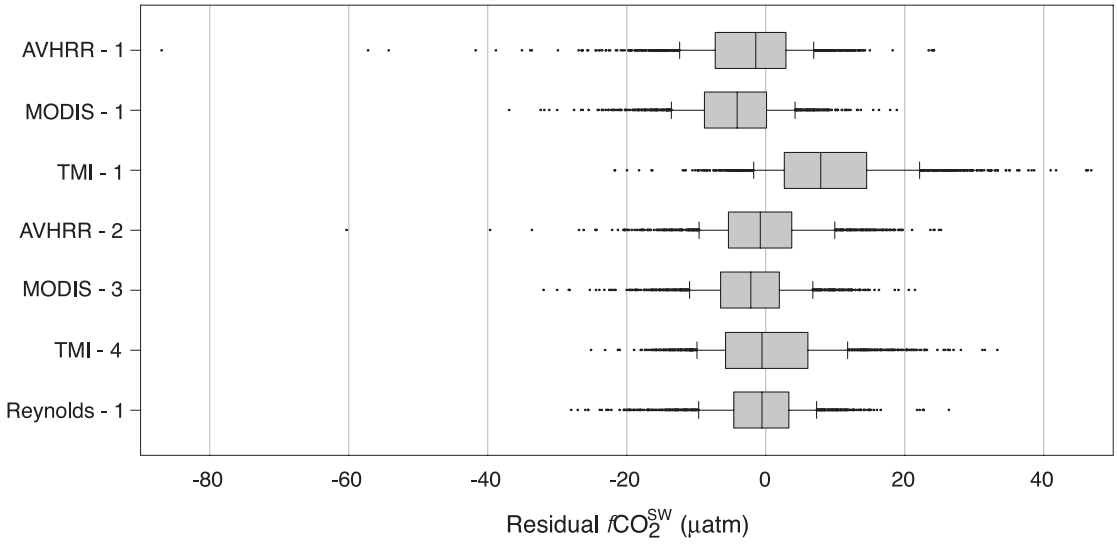

Fig. 5. Box plots of residuals between fCO_2^{sw} determined from remotely sensed SST data and bin-averaged fCO_2^{sw} data from the *Explorer*. Resolution 0.5° lat × 0.5° lon × 1 week. The line within each box indicates the median residual, the boundaries indicate 25th (closest to zero) and 75th percentile, and the whiskers indicate 10th and 90th percentiles. The name of each box is the SST field and number of the equation used to compute the fCO_2^{sw} fields.

Table 2
Summary of statistics of the residuals between computed fCO_2^{sw} and bin-averaged fCO_2^{sw} data from the *Explorer* (in µatm)

	AVHRR–Eq. (1)	MODIS–Eq. (1)	TMI–Eq. (1)	AVHRR–Eq. (2)	MODIS–Eq. (3)	TMI–Eq. (4)	Reynolds–Eq. (1)
10th Quartile	−12	−14	−1.7	−9.6	−11	−9.8	−9.7
Median	−1.4	−4.1	7.9	−0.78	−2.1	−0.53	−0.55
90th Quartile	6.9	4.2	22	9.9	6.7	12	7.3
Mean	−2.3	−4.5	9.1	−0.56	−2.2	0.40	−0.92
S.D.	8.3	7.0	8.4	7.9	7.0	8.6	6.9

For the regression with SST from the TMI using collocation criteria of less than 4.5 km and less than 6 h:

$$fCO_2^{sw} = 6.440\ (\pm 0.2) \times SST_{TMI} + 0.03480\ (\pm 0.2) \times \text{lat} - 0.5533 \pm (0.05) \times \text{lon} + 142.2\ (\pm 6)$$
$$n = 927,\ r^2 = 0.66,\ \text{rms} = 9.5\ \mu atm. \quad (4)$$

If lat and lon are excluded from the algorithms, the rms increases by 6.2–10.1 µatm.

The sensitivity to SST depends on the source of the SST data, it is highest when the shipboard data are used, and lowest when the TMI data are used. This is attributed to the larger scatter in the remotely sensed SST data (see Figs. 2–4).

Weekly fields of fCO_2^{sw} in the Caribbean Sea were computed by using Eqs. (1)–(4) on remotely sensed SST data. Table 1 shows the different permutations of fCO_2^{sw}–SST relationships and remotely sensed SST data. All calculations were carried out on a 0.5° lat × 0.5° lon × 1 week resolution. Depending on the resolution of the remotely sensed SST product, data were either interpolated or bin-averaged to fit the grid. The AVHRR and MODIS data were bin-averaged. The TMI SST were interpolated from the daily 25 × 25 km grid to a daily 0.5° lat × 0.5° lon grid and averaged over each week, and the Reynolds SST product was resampled from the original 1° lat × 1° lon grid to the 0.5° lat × 0.5° lon grid. Grid cells lacking data were filled using spline interpolation of data from surrounding cells.

The fields were computed for the region bound by 15°N, 90°W; 30°N, 90°W; 30°N, 60°W; and 15°N, 60°W.

2.4. Evaluation of computed fCO_2^{sw} fields

The computed fields were compared with the measured fCO_2^{sw} data. This was carried out by first averaging the measured fCO_2^{sw} values obtained along the cruise track into bins of size 0.5° lat × 0.5° lon × 1 week, i.e. same grid resolution as the fields estimated above, giving a total of 1648 bins. The difference between fCO_2^{sw} computed from the fCO_2^{sw}–SST relationship and the averaged measured fCO_2^{sw} values in each of the bins containing any measurements was then calculated. Box plots of these residuals are shown in Fig. 5, and the relevant statistics are listed in Table 2.

When fCO_2^{sw} is computed from either the AVHRR, MODIS, or TMI SST data and Eq. (1), the resulting values are biased. Both AVHRR and MODIS data yields lower fCO_2^{sw} values than measured, while TMI yields too high values. Using the equation based on SST data from the respective sensor yields essentially unbiased fCO_2^{sw} values for the AVHRR and TMI data. There is still a negative bias in the fCO_2^{sw} values computed from MODIS data but it is reduced relative to the bias of the fCO_2^{sw} data computed by applying Eq. (1) on the MODIS data. The application of Eq. (1) on the Reynolds SST fields also produces fairly unbiased fCO_2^{sw} values and these values appear most precise. Thus, either of the combinations AVHRR–Eq. (2), TMI–Eq. (4), and Reynolds–Eq. (1) produces good fCO_2^{sw} values compared to in situ data with a mean residual of less than 1 µatm. Evaluating the seasonal evolution of the residuals (Fig. 6) reveals that the accuracy of the fCO_2^{sw} values computed using the AVHRR–Eq. (2) and TMI–Eq. (4) algorithms depends on season. During spring these tend to overestimate fCO_2^{sw} and during summer fCO_2^{sw} is underestimated. This is a consequence of the lower sensitivity to SST variability of Eqs. (2) and (4) compared Eq. (1). Thus the combination of Reynolds SST fields and Eq. (1) produces the most accurate estimate throughout the whole year and will be used for the calculation of the sea–air CO_2 flux.

An additional and independent validation of this procedure was comparing computed fCO_2^{sw} values with fCO_2^{sw}

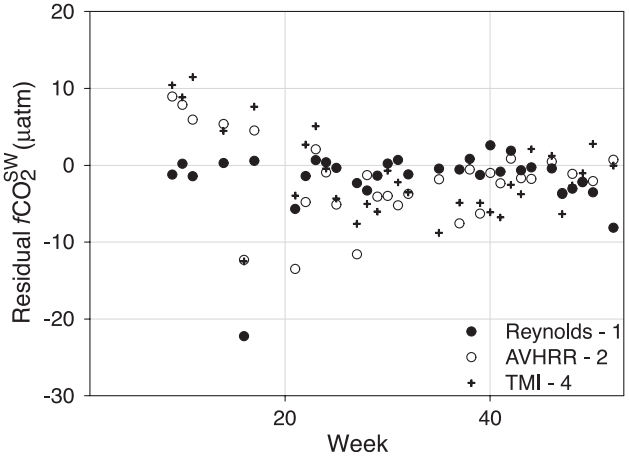

Fig. 6. Weekly mean residuals between fCO_2^{sw} determined from remotely sensed SST data and bin-averaged fCO_2^{sw} data from the *Explorer*. The name of each symbol type is the SST field and number of the equation used to compute the fCO_2^{sw} fields.

data obtained at the NOAA vessel *R/V Ronald H. Brown* in the study region in 2002. The positions are shown in Fig. 7, there are a total of 6325 measurements, mostly in the northern and eastern part of the study area. The data have been obtained in January, March, May, June, August, and October. When bin-averaged to fit the resolution of the computed fCO_2^{sw} data, a total of 214 bins were obtained. Fig. 8 shows box plots of the residual of fCO_2^{sw} and SST. The computed fCO_2^{sw} values reproduce the measured with little or no bias, and the occurrence of outliers in fCO_2^{sw} is associated with SST outliers. This suggests that the method is robust when compared to independent data, and that it can be safely applied also to the eastern part of the study area.

Comparing bin-averaged fCO_2^{sw} from both the *Explorer* and *Brown* with the fCO_2^{sw} estimated using Reynolds SST fields and Eq. (1) gave a mean residual of -0.95 μatm with a standard deviation of 7.0 μatm, this latter value is taken as a measure of the precision of the calculated fCO_2^{sw} values.

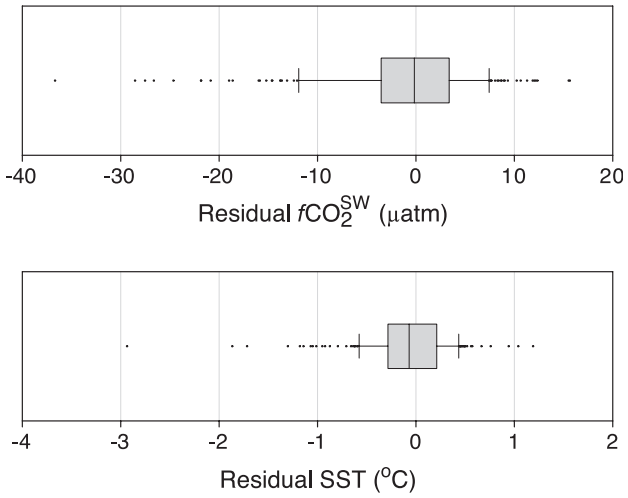

Fig. 8. The upper panel shows box plot of residuals between fCO_2^{sw} determined using Reynolds SST and Eq. (1) and bin-averaged fCO_2^{sw} data from the *Brown*. The lower panel shows box plot of residuals between Reynolds SST and bin-averaged SST data from the *Brown*. Resolution 0.5° lat × 0.5° lon × 1 week.

2.5. Estimation of sea–air CO_2 flux fields

The sea–air CO_2 flux, F, was calculated according to:

$$F = K_0 \times k \times (fCO_2^{atm} - fCO_2^{sw}) \quad (5)$$

where K_0 is the solubility, k is the transfer velocity for sea–air CO_2 exchange, and fCO_2^{atm} and fCO_2^{sw} are the atmospheric and sea surface fCO_2, respectively. Following the analysis of Section 2.4, fields of fCO_2^{sw} were computed from Reynolds SST fields and Eq. (1). Solubility was calculated according to Weiss (1974) using the Reynolds SST fields and climatological salinities from the World Ocean Atlas 2001 (Conkright et al., 2002). The SST and salinity fields were resampled from the original 1° lat × 1° lon grid to the 0.5° lat × 0.5° lon grid employed in the present work using a triangle based cubic spline interpolation. The transfer velocity was computed using measurements of wind speed obtained at a spatial resolution of 25 km by the SeaWinds sensor on QuikSCAT. This sensor is a microwave radar and the retrieval algorithms provide wind speed and direction at a height of 10 m over the ocean surface. In this work, we use the Level 2B wind vector data provided by the Physical Oceanography Distributed Active Archive Center of JPL at http://podaac.jpl.nasa.gov. Following Wanninkhof, Doney, Takahashi, and McGillis (2002), weekly mean transfer velocities at 0.5° lat × 0.5° lon resolution were computed according to:

$$k = 0.31 \times \frac{\sum U_{10}^2}{n} \times \left(\frac{Sc}{660}\right)^{-\frac{1}{2}} \quad (6)$$

where U_{10} is the individual wind speed measurements, n is number of U_{10} retrievals in each 0.5° lat × 0.5° lon × 1 week grid cell (typically around 40–50), and Sc is the

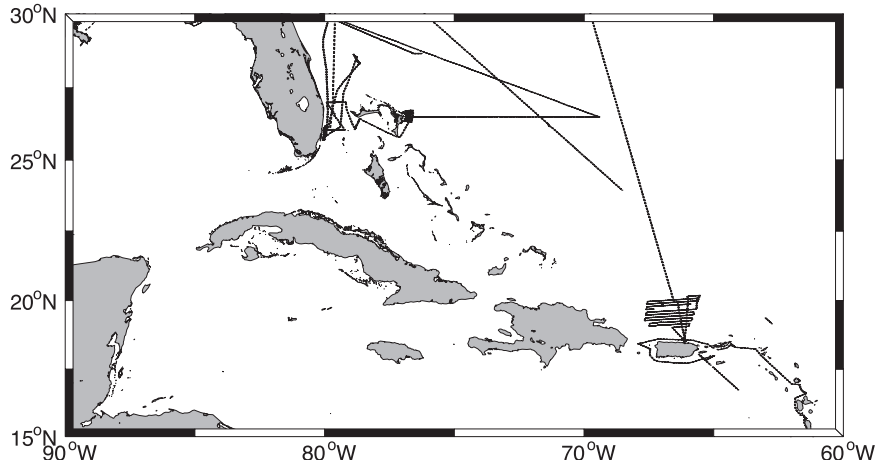

Fig. 7. The location of *R/V Ronald H. Brown* in the study area in 2002 where the fCO_2^{sw} validation data were obtained.

Schmidt number computed according to Wanninkhof (1992) from the interpolated Reynolds SST fields.

pCO_2^{atm} was computed according to:

$$pCO_2^{atm} = XCO_2(SLP - pH_2O) \quad (7)$$

Data for the dry atmospheric mole fraction of CO_2 (XCO_2) in 2002 were made available by the NOAA/CMDL Carbon Cycle Greenhouse Gases Group flask sampling program (T.J. Conway, personal communication, 2003). Monthly mean values from Key Biscayne, Florida (25.7°N) and Ragged Point, Barbados (13.2°N) were linearly regressed to obtain the latitudinal gradient of XCO_2. Gridded fields of daily mean sea level pressure (SLP) for 2002 were obtained from the NOAA-CIRES Climate Diagnostics Center, Boulder, CO, USA, from their web site at http://www.cdc.noaa.gov/, and originate from the NCEP/NCAR reanalysis project (Kalnay et al., 1996). The SLP data were supplied on an approximately 2.5° lat × 2.5° lon grid, and were re-gridded using a triangle based cubic spline interpolation and averaged to fit the 0.5° lat × 0.5° lon × 1 week grid of the fCO_2^{sw} fields. Water vapor pressure, pH_2O, was calculated from Reynolds SST according to Cooper, Watson, and Ling (1998). pCO_2^{atm} were converted to fCO_2^{atm} by assuming a 0.3% decrease from the pCO_2^{atm} value (Weiss, 1974), a procedure considered sufficiently accurate for the present purpose.

The 0.5° lat × 0.5° lon landmask of Raich and Potter (1995) obtained from the Carbon Dioxide Analysis Center at http://cdiac.esd.ornl.gov/ was used to identify land covered pixels.

3. Seasonal and spatial variability of sea–air flux of CO_2 in the Caribbean Sea in 2002

Seasonal mean maps of fCO_2^{sw}, ΔfCO_2 ($=fCO_2^{atm} - fCO_2^{sw}$), wind speed, and sea–air CO_2 flux in the Caribbean Sea 2002 are shown in Figs. 9–12. Seasons are defined as winter: January 1 to March 2 and December 1 to 31; spring: March 3 to June 1; summer: June 2 to August 31; and fall: September 1 to November 30. The gray shaded regions in (Figs. 9, 10, and 12) indicate regions at the boundaries of the domain remote from the ship tracks with no means of validating the algorithms.

In winter and spring 2002, the fCO_2^{sw} distribution showed an increase from north to south. During summer, the gradient tipped more west to east, with lowest values to the east in the Atlantic subtropical gyre. The distribution of fCO_2^{sw} in fall was characterized by a NE to SW gradient and highest values were found in the Caribbean Sea proper. fCO_2^{sw} values peaked in summer and fall. The distribution of ΔfCO_2 in 2002 followed the fCO_2^{sw} distribution. During winter the whole region was undersaturated, with CO_2 being absorbed by the ocean, except for the SW part. In spring, the pattern was the same except for oversaturation, leading to evasion of CO_2 from the ocean, to the north and east of Cuba. The whole area was oversaturated in summer and this was also the case in fall except for a small zone to the NE. The wind speeds in 2002 were fairly uniform, both in time and space with seasonal amplitude of only a few meters per second. Highest wind speeds were found to the south being around 9 m s^{-1} on average. The wind speed decreased northward, down to average values around 5–7 m s^{-1}. The distribution of the

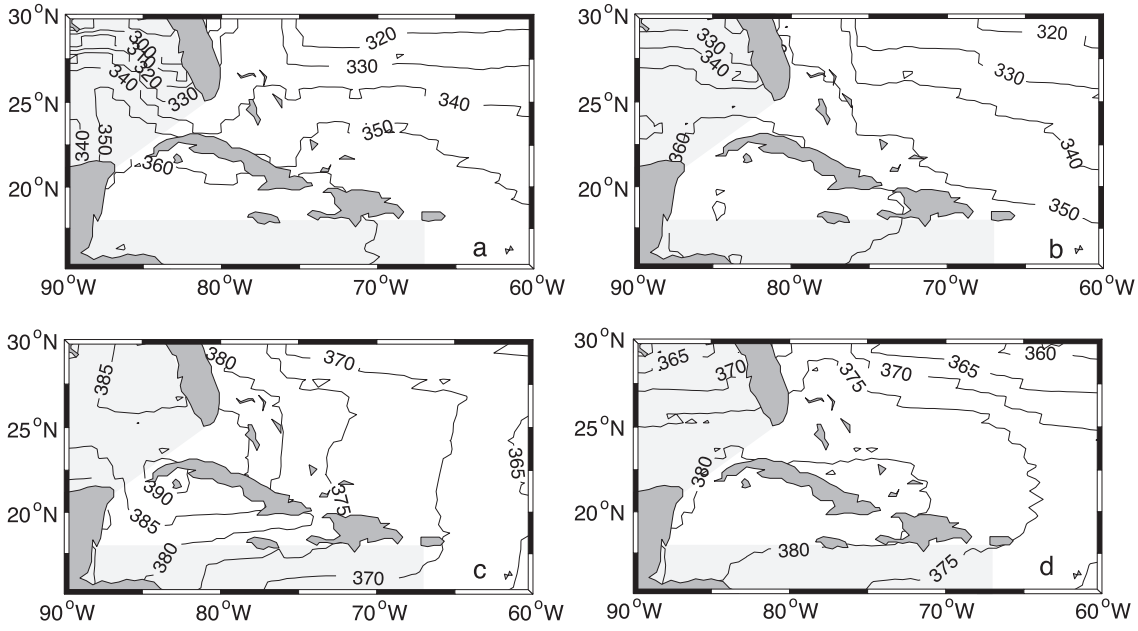

Fig. 9. Seasonal mean maps of fCO_2^{sw} (in μatm) in: winter (a), spring (b), summer (c), and fall (d), 2002. The seasons are defined as winter: January, February, December; spring: March–May; summer: June–August; and fall: September–November. The gray areas are regions where the procedure for calculating fCO_2^{sw} values has not been validated.

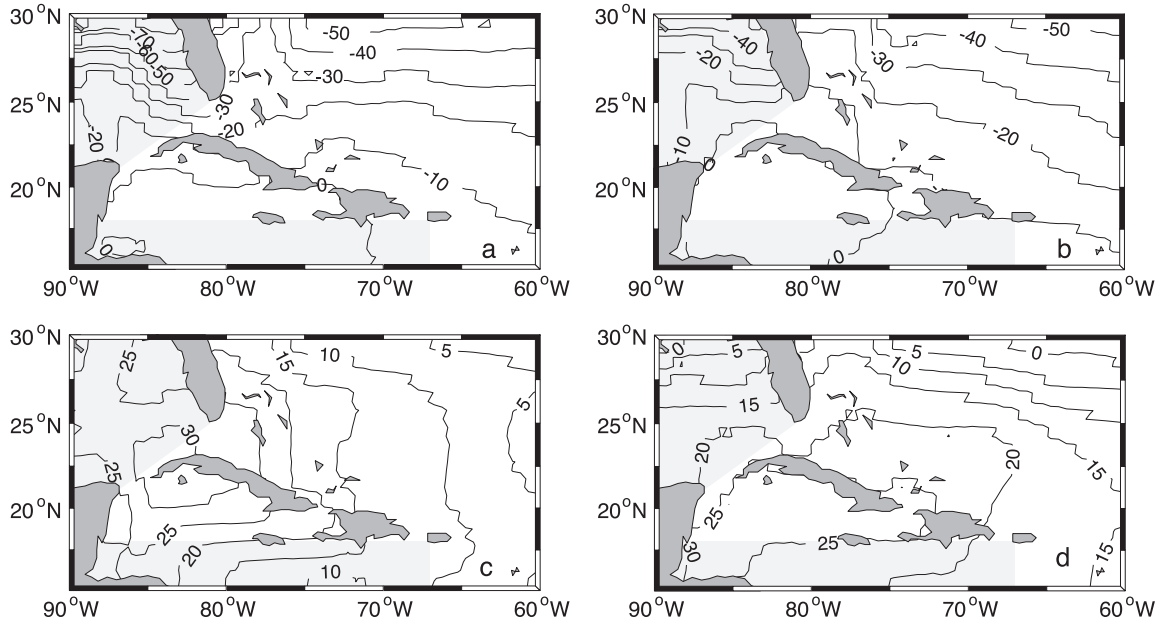

Fig. 10. Seasonal mean sea–air fCO_2 difference ($\Delta fCO_2 = fCO_2^{atm} - fCO_2^{sw}$) (in μatm) in 2002. The gray areas are regions where the procedure for calculating fCO_2^{sw} has not been validated. See caption of Fig. 9 for details.

sea–air CO_2 flux in 2002 resembles that of ΔfCO_2, but with some additional structure resulting from wind speed variability. Except for the region SW of Cuba and Hispaniola which was close to neutral, fluxes of CO_2 were into the ocean during winter. The most intense fluxes of up to -8 to -10 mmol m^{-2} day^{-1} occurred in the northern parts, in the Gulf of Mexico, and in the Atlantic subtropical gyre. The distribution was the same in spring, although ingassing was not as intense and isolines of equal flux were tipped somewhat to a NW to SE direction in the subtropical gyre. This results from the change in the fCO_2^{sw} distribution (Fig. 9). In summer, net outgassing occurred over the whole region, with intensity dropping off SW to NE. This pattern is a result of both fCO_2^{sw} and wind speed variability, as can be appreciated from Figs. 9 and 11, the fCO_2^{sw} decreased west to east while winds decreased south to north. In fall, only the northeastern parts of the region took up CO_2, and the outgassing pattern decreased SW to NE as in summer. The greatest seasonal

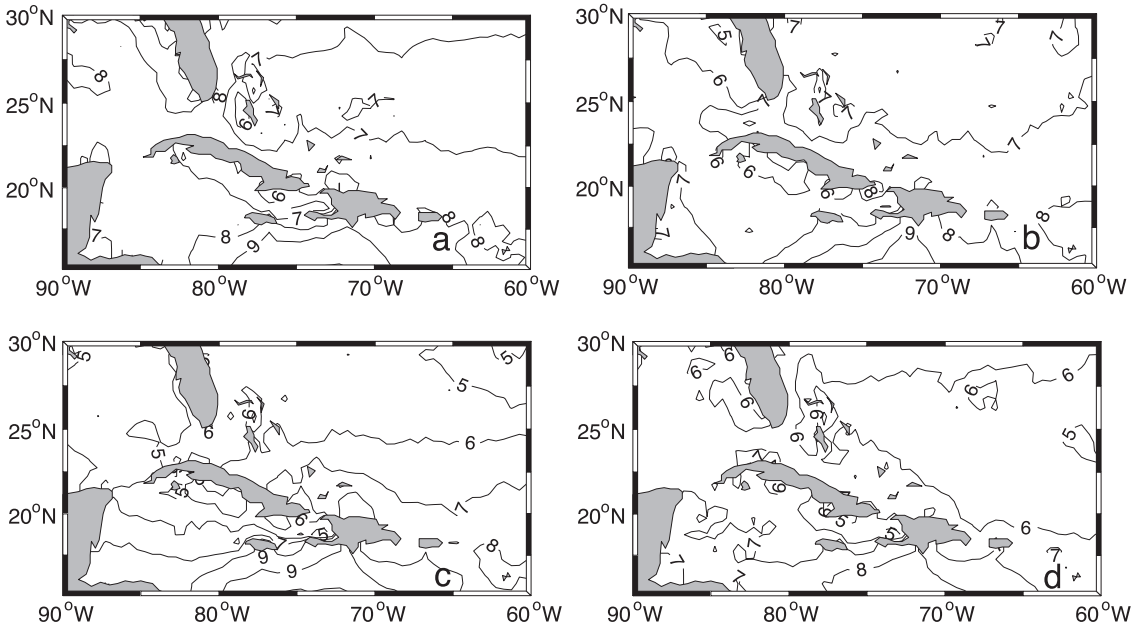

Fig. 11. Seasonal mean wind speed at 10 m above the sea surface (in m s^{-1}) retrieved by QuikSCAT in 2002. See caption of Fig. 9 for details.

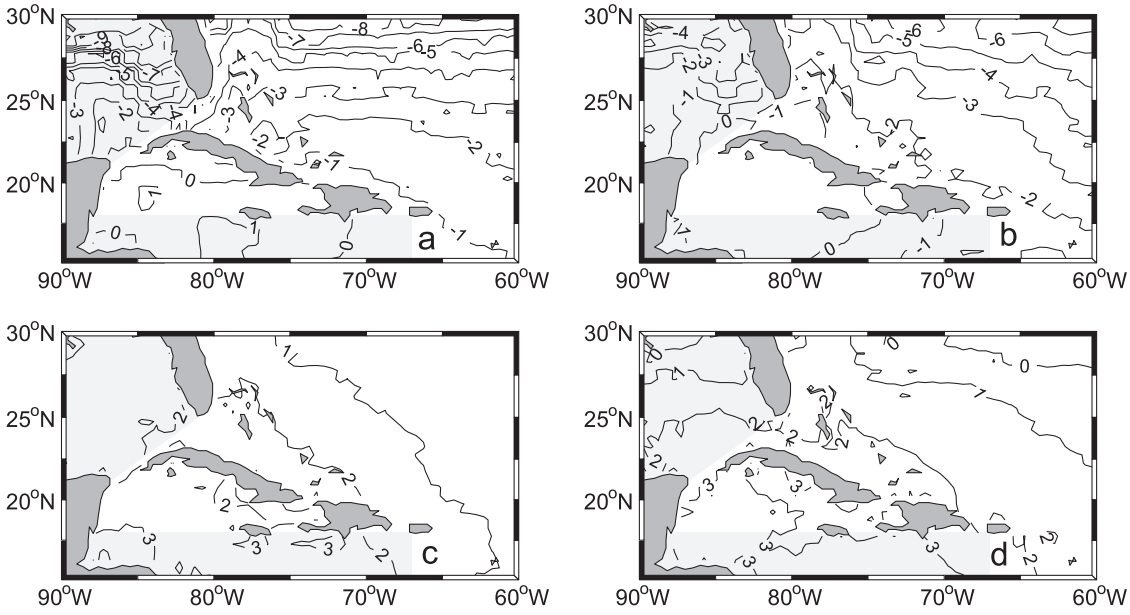

Fig. 12. Seasonal mean sea–air CO_2 flux (in mmol m^{-2} day^{-1}) in 2002. Negative values reflect a flux into the ocean. The gray areas are regions where the procedure for calculating fCO_2^{sw} has not been validated. See caption of Fig. 9 for details.

variations of the flux took place in the Atlantic subtropical gyre and in the Gulf of Mexico, while the Caribbean Sea proper exhibited the lowest seasonal changes. This reflects mainly the amplitude of the seasonal SST changes in the different parts of the study area (not shown). In the Caribbean Sea proper, SST ranged from 27 to 30 °C in 2002, while in the subtropical gyre the temperatures ranged from 23 to 29 °C. The Gulf of Mexico also heated up significantly from winter to summer and the temperature changed from around 22–23 to 29–30 °C.

Fig. 13 shows the net annual CO_2 fluxes (mol m^{-2}) in 2002. The northern and eastern parts of the study area were net annual sinks of CO_2 of around 0.5–1 mol C m^{-2}, and the southwestern parts were net sources of CO_2 of about 0.5–1 mol C m^{-2}. The border between source and sink regions followed approximately the archipelago of the Bahamas and the Antilles arc. The net annual sea–air flux amounted to an ocean uptake of 4.8×10^{11} mol or 5.7×10^{12} g of carbon into the region.

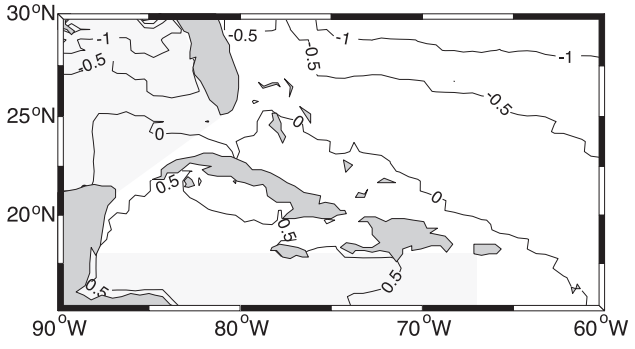

Fig. 13. Net annual sea–air CO_2 flux in 2002 (in mol m^{-2}). Negative values reflect a flux into the ocean. The gray areas are regions where the procedure for calculating fCO_2^{sw} has not been validated.

At the range of wind speeds and solubilities in the study area, the precision of the computed fCO_2^{sw} values of ± 7 μatm corresponds to an uncertainty in the weekly flux estimates of about ± 0.9 mmol m^{-2} day^{-1}.

4. Discussion

Use of remote sensing data is a powerful tool for the interpolation of surface seawater fCO_2 data. However, one must take care to ensure that the SST products used are unbiased or that they have similar bias as the SST data that the fCO_2^{sw} data are fit to. Fig. 14 shows the difference between remotely sensed SST and bin-averaged SST data from the *Explorer*. The Reynolds SST data are slightly negative biased when compared to the shipboard SST data (-0.10 ± 0.41 °C, mean and standard deviation of residuals), the TMI data are positively biased (0.88 ± 0.82 °C), and the MODIS data and AVHRR data are both negatively biased (-0.45 ± 0.40 and -0.24 ± 0.60 °C, respectively) The bias in these fields is slightly larger than the bias of the collocated data (Figs. 2–4) due to imperfections in the bin-averaged data because of insufficient data coverage. Bias in remotely sensed SST can come from several sources. It can be the result of cloud contamination or high concentrations of atmospheric aerosols (e.g. Reynolds, 1993). Satellite instruments can experience problems like for instance problematic blackbody calibration. The optimization of SST retrieval algorithms using global SST datasets makes such algorithms accurate for a global

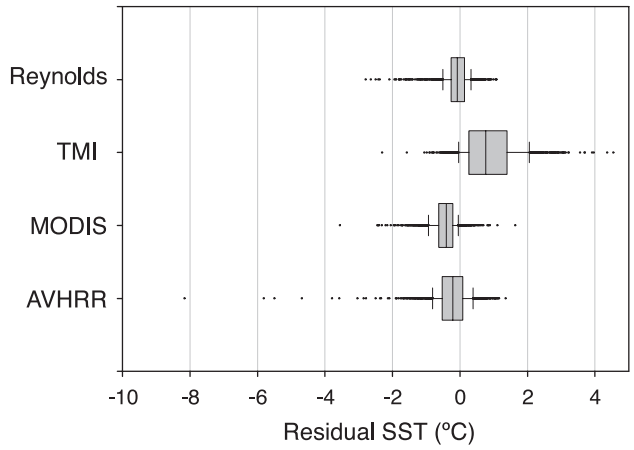

Fig. 14. Box plots of residuals between remotely sensed SST and bin-averaged SST data from the *Explorer*. Resolution 0.5° × 0.5° × 1 week.

mean atmosphere but can result in regional biases (e.g. Shenoi, 1999). The variability of the vertical temperature structure of the surface ocean i.e. skin temperature effects can effect interpretation of the signal (e.g. Keogh, Robertson, Donlon, & Nightingale, 1999). All these factors make retrieval of highly accurate SST (in the traditional sense, i.e. bulk mixed layer temperatures, 1–5 m depth) using space-borne sensors difficult, if not impossible. Following the existence of systematical biases in remotely sensed SST, significantly biased fCO_2^{sw} fields may result from uncritical application of fCO_2^{sw}–SST relationships based on shipboard data only, on fields of remotely sensed SST. In this study, use of a shipboard fCO_2^{sw}–SST relationship, Eq. (1), on MODIS, AVHRR, and TMI data yielded biases in estimated fCO_2^{sw} of -4.5 ± 7, -2.3 ± 8, and 9.1 ± 8 μatm (mean and standard deviation of residuals, Table 2), respectively. The bias in computed fCO_2^{sw} values can be reduced by using empirical fCO_2^{sw}–SST relationships derived from remotely sensed SST data collocated with the shipboard fCO_2^{sw} data. In this study, mean bias in fCO_2^{sw} computed from SST fields derived from MODIS, AVHRR, and TMI data were reduced to -2.2 ± 7, -0.6 ± 8, and 0.4 ± 9 μatm when the equation estimated using SST from the respective sensor (Eqs. (3), (2) and (4), respectively) was employed. However, the accuracy of the two latter was dependent on season and the application of the equation based on shipboard data only on the Reynolds SST data provided the most accurate fCO_2^{sw} estimates throughout the whole year. The Reynolds SST product is created from bias corrected AVHRR data. The bias correction is carried out through application of a smooth correction field generated from in situ ship and buoy SST to the AVHRR SST data, removing any large-scale satellite SST bias prior to the optimum interpolation (Reynolds & Smith, 1994; Reynolds et al., 2002). Accurate bias correction of SST requires adequate supply of in situ SST data, and while this is the case in the Caribbean Sea, coverage in remote areas such as the Southern Ocean and the northern North Atlantic is more scarce (Reynolds et al., 2002). Thus, while a shipboard fCO_2^{sw}–SST relationship applied on the Reynolds SST fields yields fairly unbiased fCO_2^{sw} estimates in the present study, this is not necessarily the case in other ocean regions. Use of shipboard fCO_2^{sw}–remotely sensed SST relationships may prove to be a better alternative in such regions.

Table 3 lists net annual CO_2 fluxes in the Caribbean Sea estimated using the different methods, and provides a quantitative measure of the effect of using shipboard fCO_2^{sw}–SST relationships on remotely sensed SST. The annual net flux is close to neutral, so it shows great sensitivity to the choice of method. When the shipboard fCO_2^{sw}–SST relationship is applied on different SST products, the flux estimates range from an annual uptake of 15×10^{12} g C to an annual release of 3×10^{12} g C. Applying the equations based on shipboard fCO_2^{sw} and remotely sensed SST narrows this range down to a net uptake between 2.0 and 8.5×10^{12} g C. The most realistic flux estimates are produced by the combinations AVHRR SST–Eq. (2), TMI SST–Eq. (4), and Reynolds SST–Eq. (1). This narrows the estimate of the net annual uptake down to between 2.0 and 5.7 10^{12} g C. Further discrimination is difficult since at this level of precision mean bias in computed fCO_2^{sw} is not directly recognized in the flux estimate illustrating that the seasonal dependence of the bias in fCO_2^{sw} becomes an issue.

4.1. Skin temperature effects

The algorithm used in the present study was optimized to reproduce fCO_2^{sw} as measured at the SST determined by the thermosalinograph that has an intake depth of 2 m. As highlighted by Robertson and Watson (1993) and Van Scoy, Morris, Robertson, and Watson (1995), sea–air CO_2 fluxes determined using such fCO_2^{sw} values may be erroneous since the flux takes place at the very surface of the ocean which is at the skin temperature, slightly colder than the bulk mixed layer. Assuming that renewal of the surface skin layer is sufficiently rapid, this effect can be accounted for by adjusting measured fCO_2^{sw} to the skin temperature instead of the temperature at the intake depth. The *Explorer* is equipped with a shipboard infrared radiometer that determines skin temperature, the Marine-Atmospheric Emitted Radiance Interferometer (M-AERI) (Minnett et al., 2001). In order to acquire an estimate of skin temperature

Table 3
Net annual sea–air flux of CO_2 in the study area (in 1×10^{12} g carbon) computed using different combinations of SST fields (rows) and equations (columns)

	Eq. (1)	Eq. (2)	Eq. (3)	Eq. (4)
AVHRR	− 13	− 2.0		
MODIS	− 15		− 8.5	
TMI	3.0			− 4.8
Reynolds	− 5.7			

effects on the sea–air flux of CO_2 in the current study area, an algorithm to retrieve fCO_2 at skin temperature, fCO_2^{skin}, from remotely sensed SST was developed. Equilibrator headspace fCO_2 values were adjusted to quality controlled skin temperature as measured by the M-AERI (see Kearns, Hanafin, Evans, Minnett, & Brown, 2000) according to the iso-chemical temperature dependency of Takahashi et al. (1993). On average, skin temperature was 0.18 ± 0.12 °C colder than SST measured by the thermosalinograph and resulting fCO_2^{skin} was 2.9 ± 1.9 μatm lower than fCO_2^{sw}. fCO_2^{skin} data were fitted to collocated AVHRR SST measurements yielding:

$$fCO_2^{skin} = 7.424\ (\pm 0.08) \times SST_{AVHRR} + 0.04161\ (\pm 0.08) \times lat - 0.5155\ (\pm 0.04) \times lon + 120.6\ (\pm 3)$$
$$n = 5020,\ r^2 = 0.69,\ rms = 10\ \mu atm. \quad (8)$$

Applying Eq. (8) on fields of SST determined by the AVHRR yielded slightly lower fCO_2^{skin} values, with a mean residual of -1.3 ± 9 μatm (not shown). However, the bias is similar to the bias in fCO_2^{sw} determined from Reynolds SST and Eq. (1). Comparing fluxes computed using fCO_2^{sw} and fCO_2^{skin} will therefore provide a fairly accurate estimate of the skin temperature effect on sea–air CO_2 fluxes in the region. Fig. 15 shows annual mean difference between the sea–air CO_2 flux computed using fCO_2^{sw} and fCO_2^{skin}. Overall values are negative, reflecting an increase of the flux into the ocean when skin temperature effects are taken into consideration. In the Gulf of Mexico, the flux into the ocean is decreased but the values in this region are questionable since computation of fCO_2^{skin} cannot be validated here. Summing the fluxes over the whole region over the year yields a net flux of -12.3×10^{12} g C which is twice as much as the flux computed using fCO_2^{sw} values. It is noteworthy that the sea–air CO_2 flux determined using fCO_2^{sw} minus 2.9 μatm, which is the mean effect of skin temperature on fCO_2^{sw}, yields a similar ocean uptake, 12.8×10^{12} g C. This suggests reasonably homogeneous differences in skin and bulk temperature in the region.

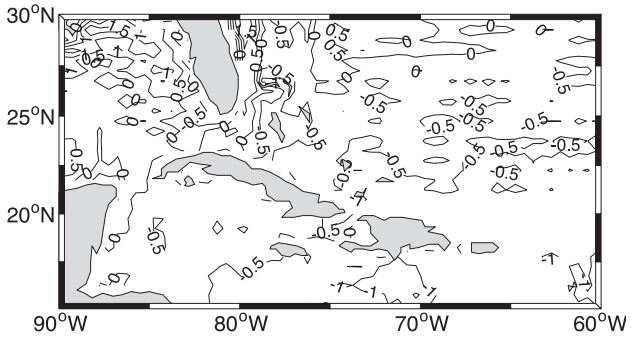

Fig. 15. Annual mean of difference between the sea–air flux computed using fCO_2^{sw} and fCO_2^{skin} (mmol m^{-2} day^{-1}).

Skin layer effects also explain some of the bias in the MODIS SST data. While the algorithm for deriving the CoastWatch AVHRR SST data is based on comparison with buoy temperature measurements, the algorithm for deriving SST from MODIS measurements is based on comparisons with measurements from buoys with an empirical correction to a skin temperature derived from M-AERI measurements. Thus, the SST data from this platform are measurements of the skin temperature and a certain bias in MODIS SST with respect to shipboard SST measured from an intake at some depth is expected. The present comparison of shipboard SST data with M-AERI skin temperature measurements and collocated MODIS SST data revealed that the two latter both were biased low with respect to the former, 0.18 and 0.30 °C (Sections 4.1 and 2.3, respectively). Thus with respect to skin temperature determined in situ with the M-AERI instrument MODIS data are biased low by ~0.1 °C.

4.2. Diurnal variability

With the application of Eq. (5) on weekly mean transfer velocities and ΔfCO_2 values as done in the present work, any contribution to the flux due to covariation between these parameters on subweekly timescales is implicitly assumed negligible (e.g. Keeling et al., 1998). The high temporal resolution of the AVHRR (measurements four times a day) and QuikSCAT data (measurements twice a day) allow for an evaluation of this assumption. AVHRR data from the passes when the sun was more than 6° below the horizon were used for nighttime SST data, and AVHRR data from passes when the sun was more than 6° above the horizon were used as daytime SST data. Weekly fields of night and daytime fCO_2^{sw} were computed by applying Eq. (2) on weekly fields of night and daytime AVHRR data. The QuikSCAT satellite crosses over the area twice daily, at 0600 and 1800 h local time, data from the latter pass were used as a measure of daytime wind speed, and data from the former were used as a measure of nighttime wind speed. Fig. 16 illustrates the covariation between diurnal fCO_2^{sw} and wind speed variability. fCO_2^{sw} tends to be higher during day than during night by 0–10 μatm, and wind speeds tends to increase during night by typically around 0.2 ± 0.4 m s^{-1} (mean and standard deviation). The daytime increase in fCO_2^{sw} is a consequence of the formation of a warm surface layer during daytime following solar heating. As shown by Gentemann, Donlon, Stuart-Menteth, and Wentz (2003), diurnal temperature changes in the region are usually around 0.6 °C and the present data exhibited a similar diurnal variability in SST (not shown), giving rise to the diurnal fCO_2^{sw} variability evident in Fig. 16. Also, in situ observations in the Sargasso Sea have revealed diurnal variations in fCO_2^{sw} of similar magnitude (Bates, Merlivat, Beaumont, & Christine Pequinget, 2000) as we observe. The diurnal variability in wind speed is associated with

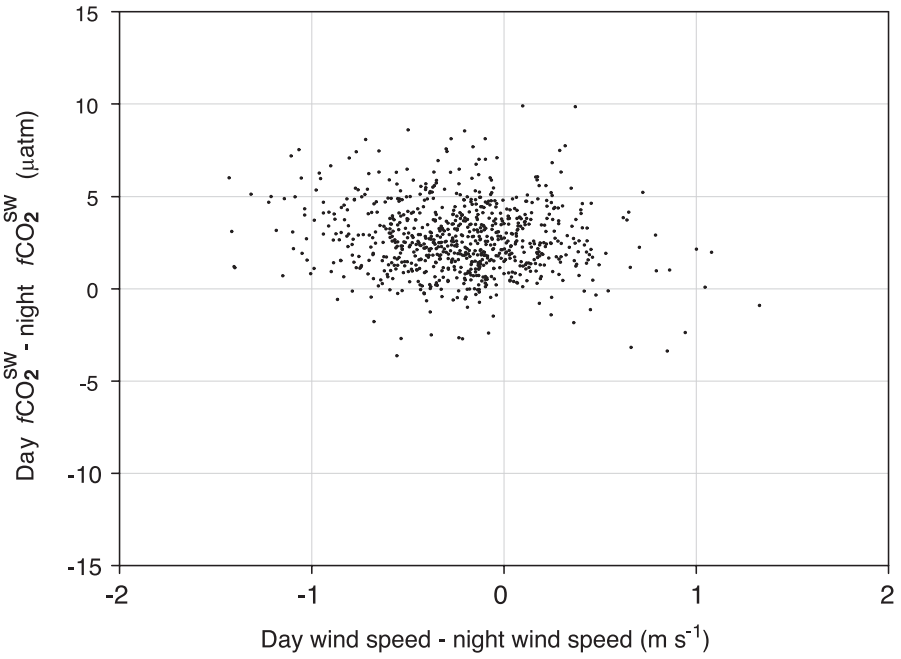

Fig. 16. Weekly mean daytime fCO_2^{sw} – weekly mean nighttime fCO_2^{sw} plotted as a function of weekly mean daytime wind speed – weekly mean nighttime wind speed. See text for how the day and night fields were computed. Each data point is the average of 1000 values.

sea breezes that occur along coastlines. Gille, Llewellyn Smith, and Lee (2003) determined diurnal wind speed variability using QuikSCAT data. For our study area, they found that wind speed as measured at morning passes were on average 0.5–1 m s^{-1} higher than during the evening passes, which is consistent with the present results. In order to evaluate the magnitude of the effect of the covariation of diurnal fCO_2^{sw} and wind speed changes, the night and day sea–air CO_2 fluxes were determined. The computations were carried out as in Section 2.4, but were done separately for day- and nighttime data, except for fCO_2^{atm}. Weekly fields of night- and daytime fCO_2^{sw} were computed from the AVHRR SST data and Eq. (2). Summing the fluxes in 2002 over the region over a year yielded a total nighttime flux of -2.63×10^{12} g C and a daytime flux of 0.663×10^{12} g C. Thus the Caribbean Sea is a net annual source of CO_2 during day and a sink during night. Summing the night and day time fluxes yields a net annual flux of -1.96×10^{12} g C which is essentially the same as the flux computed using weekly mean AVHRR data and Eq. (2). Thus, even though there is clear covariation between diurnal wind speed and fCO_2^{sw} variability in the Caribbean Sea, the effect of this on the sea–air CO_2 flux is small. This is because the diurnal wind speed variability is not of sufficient magnitude to, on its own, create diurnal variability in the air–sea CO_2 flux.

No diurnal variations were evident in the fCO_2^{sw} and SST data from the *Explorer*, because of the depth of the intake and surface mixing caused by the movement of the ship. Moreover, any variations would be hard to detect because of the lack of measurements from any given position over a whole diurnal cycle.

4.3. Computation of the sea–air CO_2 flux using monthly resolution

Estimates of the sea–air CO_2 flux over larger regions are normally carried out on a monthly basis. To evaluate if this is sufficient in the Caribbean Sea the sea–air CO_2 flux was determined on a monthly basis. Monthly fCO_2^{sw} fields were computed from monthly Reynolds SST data and Eq. (1). The monthly Reynolds SST data were obtained from the NOAA-CIRES Climate Diagnostics Center, from their web site at http://www.cdc.noaa.gov/. The monthly mean transfer velocity was computed from synoptic QuikSCAT data in the same way as the weekly mean transfer velocities following Eq. (6). The net annual sea–air CO_2 flux computed in this way amounted to -4.32×10^{12} g C, so that the uptake is 1.4×10^{12} g, or around 30% lower than the uptake computed on a weekly basis. The decrease in the flux is due to a positive bias of fCO_2^{sw} of ~ 0.5 µatm caused by the coarse temporal resolution.

5. Conclusion and recommendations

The Caribbean Sea is a region where empirical relationships between surface ocean fCO_2 and SST can be applied to interpolate shipboard surface ocean fCO_2 measurements. Other regions include the Sargasso Sea (Nelson et al., 2001), northern North Atlantic during winter (Olsen et al.,

in press), Arabian Sea (Goyet et al., 1998), and equatorial and northern Pacific Ocean (Boutin et al., 1999; Cosca et al., in press; Stephens et al., 1995). Inclusion of, for instance, ocean color may expand the regions and seasons of application of the empirical interpolation methods.

As shown by Robertson and Watson (1993), systematic biases of 3–4 μatm in mean fCO_2^{sw} can bias the global ocean carbon uptake by 0.7 gigatons/year. With this in mind, it is clear that for large-scale applications, great care must be taken to avoid systematic biases that can result from application of empirical relationships based on shipboard data only on fields of remotely sensed SST. We have shown that this can be accomplished in two ways. Either ensure that the remotely sensed SST fields are unbiased, or use a fCO_2^{sw}–SST relationship that is computed from shipboard fCO_2^{sw} data and SST data from the same remote sensing platform as the SST fields on which the empirical relationship is applied. The latter method should be applied in regions where the available SST fields are biased.

The algorithm development focused on the accurate retrieval of fCO_2^{sw} as measured at the intake temperature, as this is the conventional parameter used for computation of large-scale sea–air CO_2 fluxes. On average fCO_2^{sw} in the surface skin layer was computed to be ~ 3 μatm lower than bulk mixed layer fCO_2^{sw}, assuming an iso-chemical dependency of fCO_2 with temperature. The net uptake of CO_2 in the region was doubled when potential skin layer effects were taken into account.

There is significant diurnal variability in fCO_2^{sw} in the region of up to 10 μatm. However, diurnal wind speed variability is small so diurnal covariation between fCO_2^{sw} and wind speed can be safely neglected in the flux calculation, although this may be an issue in other regions. Remotely sensed data allow for an evaluation of diurnal variations of wind speed and SST (Gentemann et al., 2003; Gille et al., 2003); these should be used for a systematic evaluation of the potential effect of diurnal covariation on sea–air CO_2 fluxes computed on weekly and monthly timescales.

Using monthly SST fields in this region leads to underestimation of the net annual air–sea flux by around 30%.

Acknowledgements

We would like to thank Robert D. Castle, Betty Huss, and Kevin Sullivan for keeping the fCO_2 system on board the *Explorer* running and handling the data it produces. We would like to thank Peter Minnett of the University of Miami's Rosenstiel School of Marine and Atmospheric Science for sharing the M-AERI data with us and for helpful discussions. Thanks also to Kent Hughes and Don Atwood of NOAA/NESDIS for the Ocean Carbon Watch program initiative. T.J. Conway of NOAA/CMDL supplied the atmospheric CO_2 data. Finally, we would like to thank all the institutions that have made remotely sensed data available: Remote Sensing Systems (TMI data), NOAA/NESDIS Coastwatch (AVHRR data), NASA/Goddard Earth Sciences Distributed Active Archive Center (MODIS data), Physical Oceanography Distributed Active Archive Center of JPL (QuikSCAT), NOAA/NCEP (Reynolds SST), and NOAA-CIRES CDC (monthly Reynolds and SLP data). Are Olsen's work was made possible by a grant from the Norwegian Research Council. This work was carried out while Are Olsen was at a 6-month research stay at NOAA/AOML, he appreciates partial support provided by AOML and the facilities that were put at his disposition during this time. Comments from two anonymous reviewers were appreciated and helped improve this paper. This is publication no. A29 of the Bjerknes Centre for Climate Research.

References

Bates, N. R., Merlivat, L., Beaumont, L., & Christine Pequinget, A. (2000). Intercomparison of shipboard and moored CARIOCA buoy seawater fCO_2 measurements in the Sargasso Sea. *Marine Chemistry*, *72*, 239–255.

Boutin, J., Etcheto, J., Dandonneau, Y., Bakker, D. C. E., Feely, R. A., Inoue, H. Y., Ishii, M., Ling, R. D., Nightingale, P. D., Metzl, N., & Wanninkhof, R. (1999). Satellite sea surface temperature: A powerful tool for interpreting in situ pCO_2 measurements in the equatorial Pacific Ocean. *Tellus*, *51B*, 490–508.

Conkright, M. E., Locarnini, R. A., Garcia, H. E., O'Brien, T. D., Boyer, T. P., Stephens, C., & Antonov, J. I. (2002). *World Ocean Atlas 2001: Objective analyses, data statistics, and figs., CD-ROM documentation*. Silver Spring, MD: National Oceanographic Data Center, 17 pp.

Cooper, D. J., Watson, A. J., & Ling, R. D. (1998). Variation of pCO_2 along a North Atlantic shipping route (UK to the Caribbean): A year of automated observations. *Marine Chemistry*, *60*, 147–164.

Corredor, J. E., & Morell, J. M. (2001). Seasonal variation of physical and biogeochemical features in the eastern Caribbean Surface Water. *Journal of Geophysical Research*, *106*, 4517–4525.

Cosca, C. E., Feely, R. A., Boutin, J., Etcheto, J., McPhaden, M. J., Chavez, F. P., & Strutton, P. G. (2003). Seasonal and interannual CO_2 fluxes for the central and eastern equatorial Pacific Ocean as determined from fCO_2–SST relationships. *Journal of Geophysical Research*, *108*. (doi:10.1029/2000JC000677)

Feely, R. A., Wanninkhof, R., Milburn, H. B., Cosca, C. E., Stapp, M., & Murphy, P. P. (1998). A new automated underway system for making high precision pCO_2 measurements onboard research ships. *Analytica Chimica Acta*, *377*, 185–191.

Gentemann, C. L., Donlon, C. J., Stuart-Menteth, A., & Wentz, F. J. (2003). Diurnal signals in satellite sea surface temperature measurements. *Geophysical Research Letters*, *30* (doi: 10.1029/2002GL016291).

Gille, S. T., Llewellyn Smith, S. G., & Lee, S. M. (2003). Measuring the sea breeze from QuikSCAT Scatterometry. *Geophysical Research Letters*, *30* (doi: 10.1029/2002GL016230).

Goyet, C., Millero, F. J., O'Sullivan, D. W., Eischeid, G., McCue, S. J., & Bellerby, R. G. J. (1998). Temporal variations of pCO_2 in surface seawater of the Arabian Sea in 1995. *Deep Sea Research I*, *45*, 609–623.

Hood, E. M., Merlivat, L., & Johannessen, T. (1999). fCO_2 variations and air–sea flux of CO_2 in the Greenland Sea gyre using high frequency time-series from the CARIOCA drift-buoys. *Journal of Geophysical Research*, *104*, 20571–20583.

Johns, W. E., Townsend, T. L., Fratantoni, D. M., & Wilson, W. D. (2002). On the Atlantic inflow to the Caribbean Sea. *Deep Sea Research I*, *49*, 211–243.

Kalnay, E., Kanamitsu, M., Kistler, R., Collins, W., Deaven, D., Gandin, L., Iredell, M., Saha, S., White, G., Woollen, J., Zhu, Y., Chelliah, M., Ebisuzaki, W., Higgins, W., Janowiak, J., Mo, K. C., Ropelewski, C., Leetmaa, A., Reynolds, R., & Jenne, R. (1996). The NCEP/NCAR reanalysis project. *Bulletin of the American Meteorological Society*, *77*, 437–471.

Kearns, E. J., Hanafin, J. A., Evans, R. H., Minnett, P. J., & Brown, O. B. (2000). An independent assessment of pathfinder AVHRR sea surface temperature accuracy using the Marine Atmospheric Emitted Radiance Radiometer (MAERI). *Bulletin of the American Meteorological Society*, *81*, 1525–1536.

Keeling, R. F., Stephens, B. B., Najjar, R. G., Doney, S. C., Archer, D., & Heimann, M. (1998). Seasonal variation in the atmospheric O_2/N_2 ratio in relation to the kinetics of air–sea exchange. *Global Biogeochemical Cycles*, *12*, 141–164.

Keogh, S. J., Robertson, I. S., Donlon, C. J., & Nightingale, T. J. (1999). The accuracy of AVHRR SST determined using shipborne radiometers. *International Journal of Remote Sensing*, *20*, 2871–2876.

Lee, K., Wanninkhof, R., Takahashi, T., Doney, S. C., & Feely, R. A. (1998). Low interannual variability in recent oceanic uptake of atmospheric carbon dioxide. *Nature*, *396*, 155–159.

Lefèvre, N., & Taylor, A. (2002). Estimating pCO_2 from sea surface temperatures in the Atlantic Gyres. *Deep Sea Research I*, *49*, 539–554.

Li, X., Pichel, W., Clemente-Colón, P., Krasnopolsky, V., & Sapper, J. (2001a). Validation of coastal sea and lake surface temperature measurements derived from NOAA/AVHRR data. *International Journal of Remote Sensing*, *22*, 1285–1303.

Li, X., Pichel, W., Maturi, E., Clemente-Colón, P., & Sapper, J. (2001b). Deriving the operational nonlinear multichannel sea surface temperature algorithm coefficients for NOAA-15 AVHRR/3. *International Journal of Remote Sensing*, *22*, 699–704.

Minnett, P. J., Knuteson, R. O., Best, F. A., Osborne, B. J., Hanafin, J. A., & Brown, O. B. (2001). Marine-Atmosphere Emitted Radiance Interferometer (M-AERI): A high-accuracy, sea going, infrared spectroradiometer. *Journal of Atmospheric and Oceanic Technology*, *18*, 994–1013.

Nelson, N. B., Bates, N. R., Siegel, D. A., & Michaels, A. F. (2001). Spatial variability of the CO_2 sink in the Sargasso Sea. *Deep Sea Research II*, *48*, 1801–1821.

Olsen, A., Bellerby, R. G. J., Johannessen, T., Omar, A. M., & Skjelvan, I. (2003). Interannual variability in the wintertime air–sea flux of carbon dioxide in the northern North Atlantic, 1981–2001. *Deep Sea Research I*, *50*, 1323–1338.

Press, W. H., Flannery, B. P., Teukolsky, S. A., & Vetterling, W. T. (1986). *Numerical recipes*. Cambridge: Cambridge University Press.

Raich, J. W., & Potter, C. S. (1995). Global patterns of carbon dioxide emissions from soils. *Global Biogeochemical Cycles*, *9*, 23–36.

Reynolds, R., & Smith, T. (1994). Improved global sea surface temperature analyses. *Journal of Climate*, *7*, 929–948.

Reynolds, R. W. (1993). Impact of Mount Pinatubo aerosols on satellite-derived sea surface temperatures. *Journal of Climate*, *6*, 768–774.

Reynolds, R. W., Rayner, N. A., Smith, T. M., Stokes, D. C., & Wang, W. (2002). An improved in situ and satellite SST analysis for climate. *Journal of Climate*, *15*, 1609–1625.

Richards, W. J., & Bohnsac, J. A. (1990). The Caribbean Sea: A large marine ecosystem in crisis. In K. Sherman, L. M. Alexander, & B. D. Gold (Eds.), *Large marine ecosystems: Patterns, processes, and yields* (pp. 44–53). Washington, DC: AAAS.

Robertson, J. E., & Watson, A. J. (1993). Thermal skin effect of the surface ocean and its implications for CO_2 uptake. *Nature*, *358*, 738–740.

Shenoi, S. C. (1999). On the suitability of global algorithms for the retrieval of SST from the north Indian Ocean using NOAA/AVHHR data. *International Journal of Remote Sensing*, *20*, 11–29.

Stephens, M. P., Samuels, G., Olson, D. B., Fine, R. A., & Takahashi, T. (1995). Sea–air flux of CO_2 in the North Pacific using shipboard and satellite data. *Journal of Geophysical Research*, *100*, 13571–13583.

Stowe, L. L., McClain, E. P., Carey, R., Pellegrino, P., Gutman, G. G., Davis, P., Long, C., & Hart, S. (1991). Global distribution of cloud cover derived from NOAA/AVHRR operational satellite data. *Advances in Space Research*, *11*, 51–54.

Takahashi, T., Olafsson, J., Goddard, J. G., Chipman, D. W., & Sutherland, S. C. (1993). Seasonal variation of CO_2 and nutrients in the high latitude surface oceans: A comparative study. *Global Biogeochemical Cycles*, *7*, 843–878.

Van Scoy, K. A., Morris, K. P., Robertson, J. E., & Watson, A. J. (1995). Thermal Skin effect and the air–sea flux of carbon dioxide: A seasonal high-resolution estimate. *Global Biogeochemical Cycles*, *7*, 253–262.

Wanninkhof, R. (1992). Relationship between wind speed and gas exchange over the ocean. *Journal of Geophysical Research*, *97*, 7373–7382.

Wanninkhof, R., Doney, S. C., Takahashi, T., & McGillis, W. R. (2002). The effect of using time-averaged winds on regional air–sea CO_2 fluxes. In M. A. Donelan, W. M. Drennan, E. S. Saltzman, & R. Wanninkhof (Eds.), *Gas transfer at water surfacesGeophysical Monograph*, (127, pp. 351–356). Washington, DC: AGU.

Wanninkhof, R., & Thoning, K. (1993). Measurement of fugacity of CO_2 in surface water using continuous and discrete sampling methods. *Marine Chemistry*, *44*, 189–201.

Weiss, R. F. (1974). Carbon dioxide in water and seawater: The solubility of a nonideal gas. *Marine Chemistry*, *2*, 201–215.

Wentz, F. J., Gentemann, C., Smith, S., & Chelton, D. (2000). Satellite measurements of sea surface temperature through clouds. *Science*, *288*, 847–850.

Williams, E., Prager, E., & Wilson, D. (2002). Research combines with public outreach on a cruise ship. *EOS*, *83* (50), 590–596.